Analysis and Design of an Interference Canceller for Collocated Radios

Anand Raghavan, *Student Member, IEEE*, Edward Gebara, *Member, IEEE*, Emmanouil M. Tentzeris, *Senior Member, IEEE*, and Joy Laskar, *Fellow, IEEE*

***Abstract*—An active interference cancellation scheme is presented to mitigate interference between Bluetooth and wireless local area network (IEEE 802.11 b) radios operating in close proximity. This method is extensible to other mutually interfering radio devices. A reference signal correlated to the original interferer is used to generate a cancellation signal by means of amplitude and phase alignment, and filtration. The filter employed emulates the coupling channel responsible for interference. An implementation of this procedure in 0.18-μm Si-complementary metal–oxide–semiconductor (CMOS) integrated-circuit (IC) technology is also presented. The circuits fabricated are tunable and are controlled by a closed-loop adaptive process including an error minimization method. The cancellation system designed achieves 15–30 dB of interference suppression for different cases. A total power of 14 mW is dissipated by the CMOS ICs designed.**

***Index Terms*—Active circuits, adaptive control, band-limited signals, interference suppression, phase shifters, spread-spectrum communication.**

I. Introduction

A STEADY growth in the assimilation of wireless networking devices into the corporate and personal environment has been seen in recent years. The increased utilization of the industrial, scientific, and medical (ISM) bands is no coincidence since most of these devices rely on the unlicensed portion of the spectrum. While sharing of the spectrum and unlicensed access benefits the end-user, thereby facilitating increased services; it raises questions about network performance in a densely populated frequency space. Lately, these questions have received recognition, and mechanisms that deter interoperability are better understood.

The existence of a wide range of commercial products based on wireless local area networks (WLANs) and wireless personal area networks (WPANs) calls the authors' attention to their coexistence concerns. Short-range remote signaling devices using the Bluetooth standard [1] and longer range wireless data devices adhering to the IEEE 802.11 b/g standard [2] are numerous and present an example of this problem. Their functions are complementary in nature, and they both use spread-spectrum communication techniques, yet, their deployment in close proximity can and often does result in mutual performance degradation. The Bluetooth environment, for instance, is analyzed and simulated with models of the medium access control (MAC) and physical layer (PHY) to predict such a performance loss in [3]. The impairment of IEEE 802.11 devices in the presence of Bluetooth interference is quantified in [4]. Bluetooth systems conforming to the specifications of IEEE 802.15 and WLAN systems utilizing IEEE 802.11 b standards both operate in the 2.4-GHz ISM band. While the former relies on a frequency-hopping spread-spectrum (FHSS) scheme, the latter may use either an FHSS or a direct-sequence spread-spectrum (DSSS) technique. Often, when operating under closely spaced conditions, the transmitted signals from these devices may collide in both time and frequency causing a reduction in the signal-to-interference ratio (SIR) at the receiver of either system. Early findings [5] indicate that performance degradation of both systems in terms of throughput is severe when the interferers are physically located within 2 m of each other, insignificant beyond 10 m, and moderate for intermediate ranges. Naturally, this is undesirable, and methods to understand and mitigate such interference form the focus of this paper.

Various methods have been suggested to combat the coexistence problem in the 2.4-GHz band, as outlined in [6]. These range from complex time-division multiple-access (TDMA) schemes that involve load-dependent queuing and scheduling algorithms to other MAC or driver layer solutions. However, most software layer approaches disallow simultaneous operation or otherwise compromise the performance capabilities of one of the transmitting systems. Since interference is a physical phenomenon associated with the wireless RF channel and is characterized and measured in the PHY layer, a solution constituted in the PHY addresses the problem nearest the source. The methods proposed in this paper are entirely PHY layer driven and do not impair the inherent abilities of either system. The cost to be paid is manifested as increased silicon and higher power consumption in the reception and decoding circuitry.

In Section II, the theoretical underpinnings of the problem are examined in brief. This, in conjunction with measured results, helps formulate the goal of this study. Subsequently, in Section III, the interference suppression system is developed by analysis of noise mechanisms. System control issues are also addressed. An implementation of this procedure using 0.18-μm Si-complementary metal–oxide–semiconductor (CMOS) integrated-circuit (IC) technology is presented in Section IV, along with results from their measurement. Alternative circuit solutions are discussed wherever feasible. Finally, in Section V, possible extensions of the proposed interference cancellation scheme to other applications are summarily discussed.

Manuscript received April 7, 2005; revised August 30, 2005.

The authors are with the Georgia Electronic Design Center, Department of Electrical and Computer Engineering, Georgia Institute of Technology, Atlanta, GA 30308 USA and also with Quellan Inc., Atlanta, GA 30308 USA (e-mail: anandr@ece.gatech.edu).

Digital Object Identifier 10.1109/TMTT.2005.859042

II. Problem Formulation

A. Theoretical Description

Bluetooth uses a Gaussian frequency-shift keying (GFSK) continuous phase modulation scheme with a modulation index of 0.3 and a bandwidth bit-period product of 0.5. A symbol rate of 1 MS/s over any of 79 RF channels in the 2.4–2.4835 GHz band makes it effectively narrow band for the purposes of our problem. The pseudorandom hopping sequence that defines the channel has a maximum hop rate of 1600 hops/s. The transmitter Gaussian filter spreads each data bit over two symbol durations, causing intersymbol interference (ISI). The transmitted power level is usually 0 dBm (1 mW), though as much as 20 dBm is allowed. WLAN devices using the IEEE 802.11 b standard operate by various modulation schemes, depending on the data rate. They may use differential binary phase-shift keying (DBPSK), differential quaternary phase-shift keying (DQPSK), or complementary code keying (CCK). The modulated data is spread by an 11-bit Barker sequence entailing a 22-MHz channel bandwidth. The transmission channel may be one of three nonoverlapping channels over the same 2.4-GHz band. A maximum transmit power of 20 dBm (100 mW) is possible. Channel overlap in time is, thus, likely. MAC layer mechanisms in each system are well documented, and further descriptions are available from various sources, such as [7].

The theory surrounding the performance criteria of an IEEE 802.11 network in the presence of Bluetooth interferers is vast, and a few key results quantifying this effect are reproduced here. Packet error rate (PER) and number of retransmissions (RT) are taken as performance parameters, and the probability of a collision is denoted as $p(C)$. A collision is said to occur when an IEEE 802.11 b packet is unrecoverable because of a Bluetooth interferer. If N packets are transmitted and γ_{PER} represents a PER threshold, it may be shown, as in [8], that

$$p[\mathrm{PER} \le \gamma_{\mathrm{PER}}] = \sum_{n=0}^{k} \binom{N}{n} p(C)^n \left[1 - p(C)\right]^{N-n} \quad (1)$$

where k is one of $[0, 1, \ldots, N]$ and $p(\cdot)$ denotes probability. Using the standard error function when N is very large, we may approximate the binomial distribution. An expected PER less than 8% is required by IEEE 802.11 b. Therefore, the probability that the network is free of impairment may be calculated by setting the PER threshold at 0.08 in (1). The threshold condition for which the WLAN network is said to be significantly impaired is somewhat arbitrary and has been previously assumed to be 0.2. As noted before, a number of RTs may be required to successfully transmit an IEEE 802.11 b packet from the access point to the station. If γ_{RT} is a threshold for RT, the probability that this is not exceeded is calculated as the geometric distribution [9]

$$p[\mathrm{RT} < \gamma_{\mathrm{RT}}] = \sum_{n=0}^{\gamma_{\mathrm{RT}}} p(C)^n \left[1 - p(C)\right] = 1 - p(C)^{\gamma_{\mathrm{RT}}}. \quad (2)$$

The mean and standard deviation of RT are easily calculated.

In evaluating the coexistence scenario, a WLAN station and access point separated by distance d_S are considered with uniformly distributed Bluetooth piconets surrounding the station. If γ_{IS} is the interference-to-signal power ratio threshold beyond which the WLAN signal is jammed, and P_{WL} and P_{BT} are the IEEE 802.11 and Bluetooth transmit powers, then

$$\Gamma = \frac{\gamma_{\mathrm{IS}} P_{\mathrm{WL}}}{P_{\mathrm{BT}}} \quad (3)$$

is the normalized interference-to-signal threshold. Further, the area $A(\Gamma, d_S, D)$ around the station within a radius D where interference occurs, is determined by methods similar to Jakes' multipath fading calculations [10]. Some mathematical deliberation is necessary [8] to show that

$$A(\Gamma, d_S) = \pi d_S^2 \exp\left[\frac{2\left(\sigma_{\mathrm{IS}}^2 - 10n\Gamma \log_{10}(e)\right)}{\left(10n \log_{10}(e)\right)^2}\right]. \quad (4)$$

This is valid in the limiting case where D is very large. Here, σ_{IS} is the standard deviation of a log-normally distributed random variable representing the interference-to-signal ratio and n is the path loss exponent of the shadowing model used to perform the calculation. Therefore, given typical values of various parameters, interference areas can be found. For instance, $P_{\mathrm{BT}} = 0$ dBm, $P_{\mathrm{WL}} = 20$ dBm, $d_S = 20$ m, an acceptable interference-to-signal ratio threshold $\gamma_{\mathrm{IS}} = -10$ dB [11], office building conditions of $2 < n < 4$, and $5 < \sigma_{\mathrm{IS}} < 11$ dB [12] yield $A(\Gamma, d_S) \approx 1\ \mathrm{m}^2$.

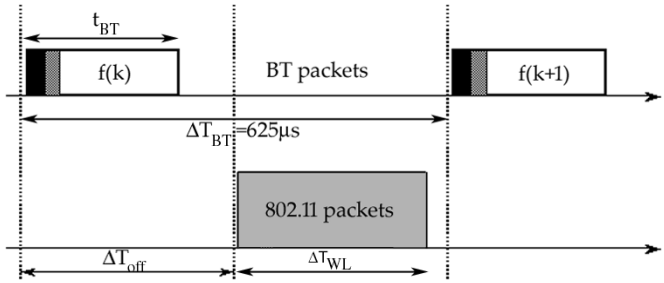

Fig. 1. Bluetooth and WLAN packet transmission timing diagram.

A simple timing diagram for packet transmission in Bluetooth and WLAN networks is shown is Fig. 1. If ΔT_{BT} is the time slot duration for Bluetooth, ΔT_{WL} is the packet transmission duration for WLAN ($\Delta T_{\mathrm{BT}} = 625\ \mu$s, $\Delta T_{\mathrm{WL}} < 1210\ \mu$s), t_{BT} is the transmission time for Bluetooth, and ΔT_{OFF} is the offset between the two transmissions, the probability of n overlaps in time between the two interfering systems is given by

$$p(n) = \frac{\left[t_{\mathrm{BT}} + \Delta T_{\mathrm{WL}} - (n-1)\Delta T_{\mathrm{BT}}\right]}{\Delta T_{\mathrm{BT}}}. \quad (5)$$

The probability of frequency collisions is similarly calculable. Finally, if the probability of activity in a single Bluetooth piconet $p(A)$ is assumed to be independent and identically distributed for all piconets, and N is the expected number of Bluetooth interferers with an interference level Γ, then the total probability of time–frequency collisions is derived [8] as

$$p(C) = \sum_{n=0}^{N} \binom{N}{n} p(A)^n \left[1 - p(A)\right]^{N-n} p(C_n) \quad (6)$$

$$p(C_n) = \sum_{k=1}^{L} \left[1 - \left[1 - p(C_1|\Gamma_k)\right]^n\right] p(\Gamma_k) \quad (7)$$

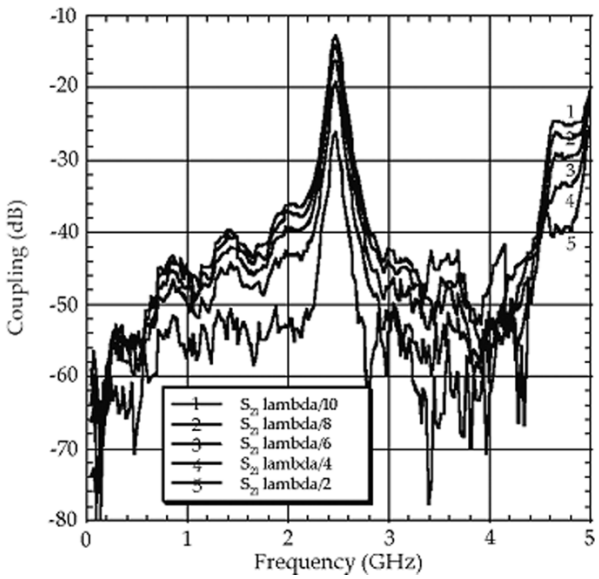

Fig. 2. Coupling characteristics between closely spaced antennas.

where L is a loading factor for the Bluetooth piconets. Hence, we may infer that for typical values of parameters noted before and path loss exponent (n) of 4, the probability of collision is greater than 10% for networks with light Bluetooth traffic and greater than 40% for networks with heavy Bluetooth traffic. Interference is, thus, a pressing concern.

B. Measurement and Characterization

Since the goal of this paper is separate from the derivation of closed-form analytical solutions to the interference problem, a practical case will be examined. Situations where multiple radio transceivers are located on the same platform in communication products are increasingly prevalent. In the special case that both radios are collocated and required to operate simultaneously from the same device, the Bluetooth transmitters are well within the interference area of the WLAN receiver as described in the previous analytical treatment of the problem. To demonstrate this, various paired patch antenna structures were fabricated on FR-4 material. These were characterized for operation in the 2.4-GHz band and able to transmit IEEE 802.11 b/g and Bluetooth data. The antennas were separated on the board by distances ranging from $\lambda/2$ to $\lambda/10$, where λ is the wavelength of the carrier radiation. These correspond to distances less than 0.1 m at 2.4 GHz, implying that the likelihood of interference is very high and the severity enough to compromise the successful recovery of desired data. The characteristics of the electromagnetic radiation between the antennas were measured and the S-parameters are plotted in Fig. 2. The plot shows the coupling between the two antennas for different spacing conditions.

As evidenced by the graph, the coupling (or relative interference level) varies from -13 to -27 dB. Maximum coupling occurs at the $\lambda/10$ spacing as expected. Such interference levels are formidable and reduce the SIR at the target receiver. A WLAN receiver has a recommended sensitivity of -75 dBm, and numbers from -85 to -95 dBm are typical. Considering that the transmit level from a Bluetooth radio can be as high as 20 dBm (with power control) or 0 dBm, signal levels at the receiver may be drowned in a sea of noise under these conditions. For receive systems with extreme sensitivity requirements such as global positioning system (GPS), a lower power radiator in its vicinity may act as an aggressor if transmitting in the same frequency band, or even by spectral fallout.

An understanding of the nature of interference in the context of our problem is necessary for achieving any success in suppressing it. We may loosely refer to the undesired energy in the receive antenna of the victim (i.e., WLAN) system as noise. Based on this definition, the noise may be separately treated as in-band and out-of-band noise. Since the transmission frequency band of 83.5 MHz width is identical for the two radios, the in-band noise pours energy into frequencies that either transmitter may use. Whereas out-of-band noise also degrades radio performance, it may be rejected by appropriately filtering at the transmit or receive end. This is possible owing to the fact that no desired information is contained in the spectrum outside the band of interest. However, out-of-band noise is not entirely trivial for the following two reasons.

- Though a transmit channel is precisely defined, it is physically impossible to limit radiation without spreading noise into sidebands, depending on the transmit spectral mask. Sideband signals, thus, are a potential source of interference.
- Out-of-band noise at the boundary of a band is as important as noise in-band because of the nonrectangular nature of filters.

Out-of-band noise, being a minor cause for concern and peripheral to our problem, will be ignored. The nature of a PHY layer solution, therefore, depends squarely on the behavior of in-band noise. Successful negotiation of in-band noise requires further categorization of noise as broad-band (white) and band-limited (colored). Broad-band noise in the time domain is a random process of statistically uncorrelated impulse energies. This implies nondeterministic behavior and no coordination with any identifiable source. Band-limited noise, on the other hand, is deterministic in nature. It is statistically correlated in time to a particular source. Since the aggressing transmitter is the source, and the coupling channel is the means of time correlation, this deterministic noise is clearly the offshoot of an intentional signal radiation. Furthermore, the in-band noise may be modeled as the superposition of a broad-band and a band-limited component.

Traditionally, most high-frequency radio systems are plagued only by broad-band noise. As such, their circuit implementations are designed to alleviate white noise only. To minimize confusion, the band-limited component of in-band noise will henceforth be referred to as the "interferer." The interference cancellation scheme suggested in this paper allows us to suppress the above-mentioned interferer while maintaining adequate broad-band noise performance. The analytical background of the scheme along with the description of a system to implement it is discussed in the following section.

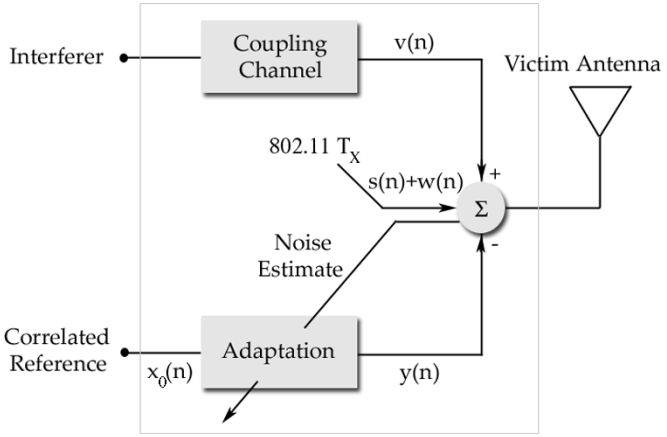

Fig. 3. Adaptive noise suppression scheme processing discrete-time signals and noise.

III. System Analysis

A. Cancellation Approach

The interference cancellation method employed by us relies on subtracting an internally generated interferer from the signal received at the victim antenna. When the subtraction and intermediate filtration is done adaptively, superior signal-to-noise ratio (SNR) may be obtained compared to direct filtration of the received signal [13]. As such, it is a dual-input closed-loop adaptive noise suppression scheme. A schematic, representative of the cancellation process, is shown in Fig. 3.

Referring to the figure, the victim antenna receives a signal

$$x(n) = s(n) + v(n) + w(n) \tag{8}$$

where $s(n)$ is the information-bearing signal of interest, $v(n)$ is a narrow-band interferer, and $w(n)$ is broad-band noise. The two noise terms are not correlated to the signal or to each other. Specifically, the expectation

$$E\left[s(n)v(n-k)\right] = 0 \tag{9}$$

for all k.

The cancellation unit receives another input $x_0(n)$ that is given by

$$x_0(n) = v_0(n) + w_0(n) \tag{10}$$

where $v_0(n)$ and $w_0(n)$ are narrow-band and broad-band noise terms, respectively. Whereas, the two broad-band noise terms are uncorrelated to any source by definition, and $v_0(n)$ is uncorrelated to the signal $s(n)$, the two narrow-band noise terms are correlated to each other. All signals under consideration are wide-sense stationary. In general, the cross correlation between the two narrow-band noise terms is unknown and given by

$$\rho(k) = E\left[s(n)v_0(n-k)\right] \tag{11}$$

for a lag k. Traditionally, $x_0(n)$ is processed by an adaptive filter to produce an output signal

$$y(n) = \sum_{k=0}^{M} g_k(n)x_0(n-k) \tag{12}$$

where $g_k(n)$ represents the adaptable weights of the filter. The output of the cancellation unit is, thus, the error signal

$$\varepsilon(n) = x(n) - y(n) = s(n) + v(n) + w_t(n) - y_0(n) \tag{13}$$

where $y_0(n)$ is the narrow-band correlated noise contribution of $x_0(n)$ to the output, and $w_t(n)$ is the total broad-band noise at the victim antenna. If the control mechanism is able to dynamically converge and achieve cancellation, the condition

$$y_0(n) > w_t(n) - w(n) \tag{14}$$

will ensure success.

The implementation described here differs from the general case above in that the cross correlation of (11) is not completely unknown. Since the aggressor antenna, which is the source of correlated noise, is assumed to be located in the immediate proximity of the victim, the cancellation unit has access to a scaled and delayed version of $v(n)$. Though this approach may slightly affect the aggressor, it obviates the need for large and complex tapped-delay finite impulse response (FIR) filters. However, it must be noted that $v(n)$ is defined not only by the source antenna but also by the wireless coupling channel. This channel is not expressible analytically in closed form and, therefore, still needs to be emulated in order to process $x_0(n)$. Under the operating conditions considered above, measurements show that the coupling channel is largely stationary in its characteristics for a given configuration of the interferers, forming the basis for the design of a simple emulation filter. The filter is endowed with limited tunability to combat dynamic environments.

In either case discussed above, the only correlation among the inputs to the canceller being between $v(n)$ and $v_0(n)$, we may write the mean power of the output as

$$E(\varepsilon^2) = E(s^2) + E\left[(v - x_0)^2\right]. \tag{15}$$

Maximizing the output SNR, therefore, requires minimizing the left-hand side of (15). Usually, this is accomplished in adaptive filtering schemes by using gradient-descent- or random-search-based control algorithms [14]. This study utilizes a gradient descent procedure for adaptation.

Examining the above correlation chain in continuous time, and preserving the same notations as in (8)–(15), we may write

$$y_0(t) = \int_{-\infty}^{\infty} G(f)V_0(f)\exp(j2\pi ft)df \tag{16}$$

where $G(f)$ is the Fourier transform of the filter and $V_0(f)$ is that of the narrow-band noise input to the cancellation unit. This is possible only when the filter is linear and the coupling channel emulated by the filter is assumed linear time invariant. When the filter output is sampled at time $t = T$, this yields

$$|y_0(T)|^2 = \left| \int_{-\infty}^{\infty} G(f)V_0(f)\exp(j2\pi fT)df \right|^2 \tag{17}$$

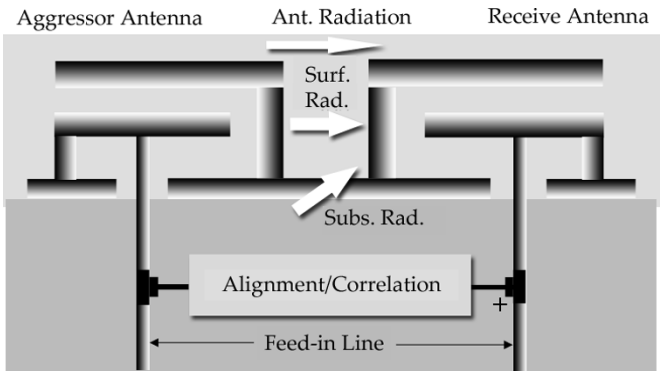

Fig. 4. Physical sources of correlated noise in a radio system and its suppression.

as the output power due to the interferer. In addition, the average power of the total broad-band noise at the victim antenna is given by

$$E\left[w_t^2(t)\right] = \frac{N_0}{2}\left[1 + \int_{-\infty}^{\infty} |G(f)|^2\, df\right] \tag{18}$$

where $N_0/2$ is the power spectral density of $w(t)$. Therefore, the SNR before and after cancellation may be expressed as

$$\mathrm{SNR}_{\mathrm{before}} = \frac{|s(T)|^2}{\left[|v(T)|^2 + E\left(w^2(t)\right)\right]}$$
$$\mathrm{SNR}_{\mathrm{after}} = \frac{|s(T)|^2}{\left[|v(T) - y_0(T)|^2 + E\left(w_t^2(t)\right)\right]}. \tag{19}$$

Here, the powers are measured at a time T, the numerators are constant, and the frequency domain representation of $y_0(T)$ is obtained from (17).

B. Proposed Canceller Unit

The cancellation technique employed, outlined earlier in [15], is schematically represented in Fig. 4. Shown here are sources of deterministic interferers acting by various physical mechanisms. The primary media responsible for crosstalk are a shared conductive substrate and air acting as a channel for antenna radiation.

A downscaled replica of the signal at the aggressing antenna is tapped off by the cancellation unit and used as the input $v_0(t)$ as in (10). The feed-in lines shown in Fig. 4 represent the transmission lines from the aggressor and victim antennas, to which the alignment/correlation chain interfaces. The alignment/correlation chain itself is responsible for emulating the aggressor signal by appropriately transforming the tapped-off input; this will be explained later. This reference input is always accompanied by the white noise $w_0(t)$ present in the aggressor and elsewhere. As long as $|v_0(t)|$ is very small compared to the transmit level in the aggressor, any effect on the Bluetooth transmission is insignificant. Coupling levels to the victim antenna being less than -13 dB, and the voltage level of the tapped-off signal needs to be less than 2.5% of the Bluetooth transmit level to accomplish cancellation with a system of unity maximum gain. A cancellation signal is generated by the unit, which is governed by external controls. Combining this signal with the received signal at the victim (i.e.., WLAN) antenna at a 180° phase differential affects the suggested interference suppression. Loop cancellation methods that are different from our method have been used before [16] to generate narrow-band nulls at specific frequencies to achieve isolation in full-duplex radios. Correlation and the generation of a cancellation signal within the unit are performed by gain and phase alignment of the input $v_0(t)$, and filtration through $G(f)$ defined in (12) and (16). An issue of significance requiring remark here is that our method creates a cancellation notch in-band that is wider compared to the above-mentioned narrow-band nulls. The method used in [16] is targeted at an adaptive duplexer in a frequency division duplex (FDD) system. In that method, two separate and independent nulls are created in the spectrum at the transmit and receive center frequencies. The two nulls separated by a 45-MHz offset are very narrow single-tone nulls. Besides, there is no overlap between the transmit and receive frequencies. However, the approach proposed in this study addresses a problem where the aggressor and source occupy exactly the same 83.5-MHz-wide band. The cancellation notch can be created over the whole band and is, thus, independent of both carrier modulation and the aggressor frequency channel in use at any given time. This is important because very-narrow-band nulls are impractical in spread-spectrum communication systems owing to their hopping nature. Furthermore, band limiting through the emulation filter helps prevent the coupled noise from decorrelating for a larger time interval, allowing easier cancellation, as suggested in [17]. Besides, as noted in [18], some applications may necessitate the use of noncausal filters in the adaptation path. Deriving the correlated input directly from the aggressor, however, negates this requirement since the interferer does not reach the victim before it does the cancellation unit. The importance of this stems from the fact that delays cannot be placed in the primary interference mechanism (air) between the Bluetooth and WLAN radios, thus, making it difficult to violate causality. This, in conjunction with the fact that the carrier frequencies are much higher than the data rates in our application, implies that interference suppression may be adequately accomplished by means of gain and phase adjustments, and filtration alone.

A prototype of the canceller was constructed on FR-4 material in keeping with the principles discussed above. A schematic is shown in Fig. 5.

The paired patch antennas of our earlier measurements act as transmitter and receiver in the problem, as illustrated in Fig. 5. Inputs to and outputs from the canceller unit are processed by power splitting and combining elements along the feed lines. The board shown is constituted of discrete components, though the IC equivalents are also described subsequently. With reference to Fig. 5, the phase aligner, variable gain amplifier (VGA), and bandpass emulation filter form the alignment/correlation chain mentioned earlier. The primary emulation filter serves as a coarse scale model of the coupling/interference channel. This

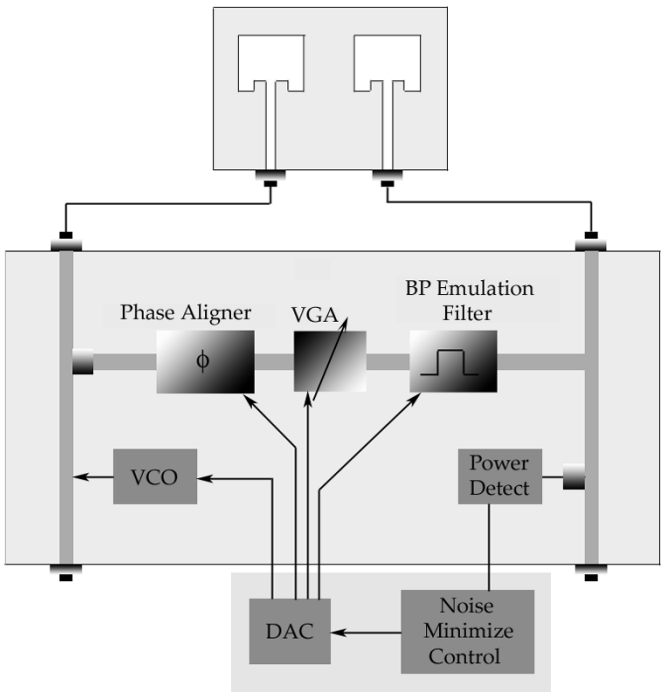

Fig. 5. Simplified schematic of the interference cancellation unit.

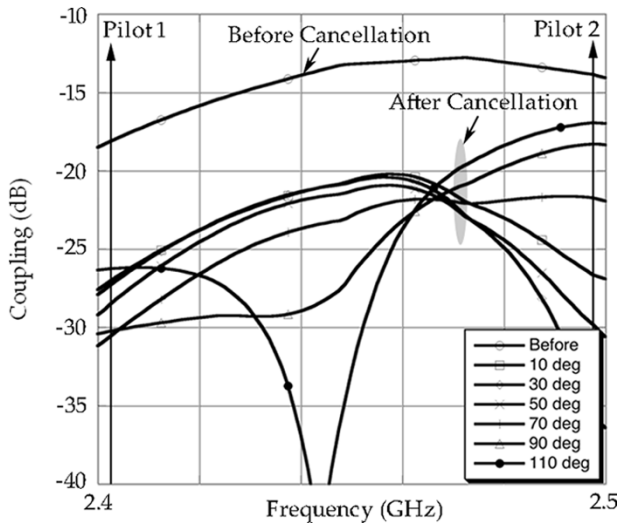

Fig. 6. Out-of-band pilot tones used for cancellation in-band by varying phase adjustment controls.

model is refined by the VGA and phase aligner to accurately match the reference input signal to the source aggressor signal, thereby correlating the two and emulating the channel.

The emulation filter is implemented as an inductance–capacitance (LC) filter with a bandpass response, so that the pass band coincides with the 83.5-MHz band of interest. It uses a varactor diode in shunt with a high-Q discrete inductor. The pass band being rather narrow in comparison with the center frequency (2441.75 MHz) necessitates the use of a high-Q inductor. Further, the varactor diode implementation of the capacitor allows voltage-controlled tunability of the filter characteristic to adjust for slight channel mismatches. Gain control is through a VGA able to provide voltage gain from 0 to 1 or greater. A 360° continuously variable phase shifter is used to align the phase of the correlated sample signal with the interferer.

External control circuitry includes a power detector to estimate the energy of the error signal, which is minimized using a feedback control loop, as indicated by the power detect and noise minimize control blocks in Fig. 5. The control loop drives several digital-to-analog converters (DACs) that adjust all the variable components. Since minimizing the error signal is equivalent to finding a minimum for the mean output signal energy as shown in (15), a relatively simple procedure is employed. Known pilot signals generated by the VCO in Fig. 5 are injected into the canceller unit along with the reference interferer. These pilots occupy extremely narrow bandwidths and are situated outside the edges of the 2.4-GHz band. Not being in-band, they do not affect canceller performance in the region of interest. It is surmised that the spectrum of the coupled signal after cancellation being smooth, a lowering of energy in-band will correspond with energy reduction at the band edge also. Hence, monitoring and minimizing the energy in the pilot signal at the output of the canceller is equivalent to minimizing coupling within the band. This, however, does not mean that the cancellation notch is wide enough to cover the whole 2.4-GHz band. Generating a wide enough notch requires simultaneously minimizing the energy of both pilots. Precise knowledge of the pilot signals and their higher power levels compared to the in-band signals makes this scheme more robust and easier to implement. The result of such a control mechanism was measured, and an example of the cancellation data within the 2.4-GHz band is shown in Fig. 6.

Various curves in the graph represent different states of the controller. As observed from the plot, a phase shift of around 90° yields optimum cancellation at one band edge (governed by pilot 1), but a different phase shift optimizes cancellation at the other edge (governed by pilot 2). The iterative error minimization process, however, selects a phase shift of around 70° as optimal for the whole band, based on both pilots. The pilots depicted in the graph are representative and not exact in power level or frequency.

The canceller features a feedback control mechanism that operates using the principle of gradient descent. Here, the controller is driven by the measured error energy gradient with respect to each control variable, after the emulation channel. During the iterative control process, the error energy describes a nonnegative error surface along which the control variables travel, depending on the adaptation algorithm used [19]. In the control loop designed, a differential steepest descent (DSD)-type algorithm [14] was used to determine the above-mentioned gradient. This is similar to the least mean squares (LMS) approach, except that unlike the latter, where the gradient is estimated during each iteration, the DSD algorithm actually calculates it.

IV. CMOS IC Implementation

The components of the canceller unit described in the previous section were implemented in a standard 0.18-μm CMOS IC technology, affording superior integrability into a radio device environment. Wireless radio front-end design migrating largely toward Si-CMOS, this offers the best possibility of

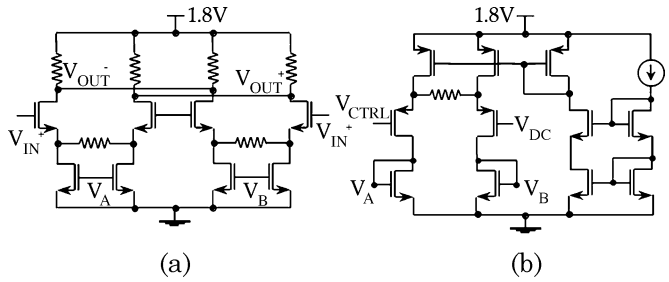

Fig. 7. (a) Simplified circuit schematic of the Gilbert-cell-based VGA. (b) Schematic of the current steering bias circuit operating the VGA with a folded cascode topology.

a low-cost compact solution. A Gilbert-cell-based VGA is designed to allow amplitude adjustment of the canceller input signal. Phase alignment is made possible by designing a continuously variable analog active phase rotator with 180° of phase range. Since the VGA is capable of shifting the input signal by a fixed phase difference of 180°, a total range of 360° is available. All circuits operate from a 1.8-V supply and are designed for a broad-band frequency response. The on-chip circuitry is driven differentially by an external balun and is matched to a 50-Ω single-ended impedance. At the output, for test purposes, a driver amplifier is used to buffer the circuitry from the 50-Ω load while matching to it.

A simplified circuit schematic of the VGA is depicted in Fig. 7(a). A simple Gilbert cell current-steering transconductor is adequate to satisfy our low maximum gain requirements. It consists of two differential pairs that amplify the input by opposite gains and summing currents that vary in opposite directions while maintaining a constant total. In contrast to typical mixed signal broad-band designs, the input and output voltage waveforms are not rail–rail swinging square pulses, but rather modulated sinusoids. Therefore, nonlinearity in the operating bias range of the Gilbert cell needs to be minimized. Resistive degeneration is used to this end. Sustaining cancellation at Bluetooth transmission levels of up to 10 dBm, the circuits operate without saturating at voltage levels of over 150–200 mV. Furthermore, the total current in the Gilbert cell, which is constant at all times, is obtained by a folded cascode differential biasing circuit as shown in Fig. 7(b). This circuit is, again, a differential pair so that the total current in its two branches remains fixed as they vary in opposite directions with changing control voltage V_{CTRL}. The differential pair has been modified using positive-channel metal–oxide–semiconductor (PMOS) transistor loads to operate as a folded cascode circuit to reduce voltage headroom demands on the VGA.

Voltage headroom is, thus, not a cause for concern. A pair of differential control voltages, one of which is fixed at a reference voltage for easy control, may operate the current biasing circuit. In order to linearize the characteristic of VGA gain against control voltage, the biasing circuit is also degenerated.

The total delay through the VGA was approximately 40 ps at 2.4 GHz, and phase variation with control voltage was minimal. The S-parameters of the VGA were measured using a four-port network analyzer. Time-domain measurements were also performed. Shown in Fig. 8(a) is the gain response of the VGA

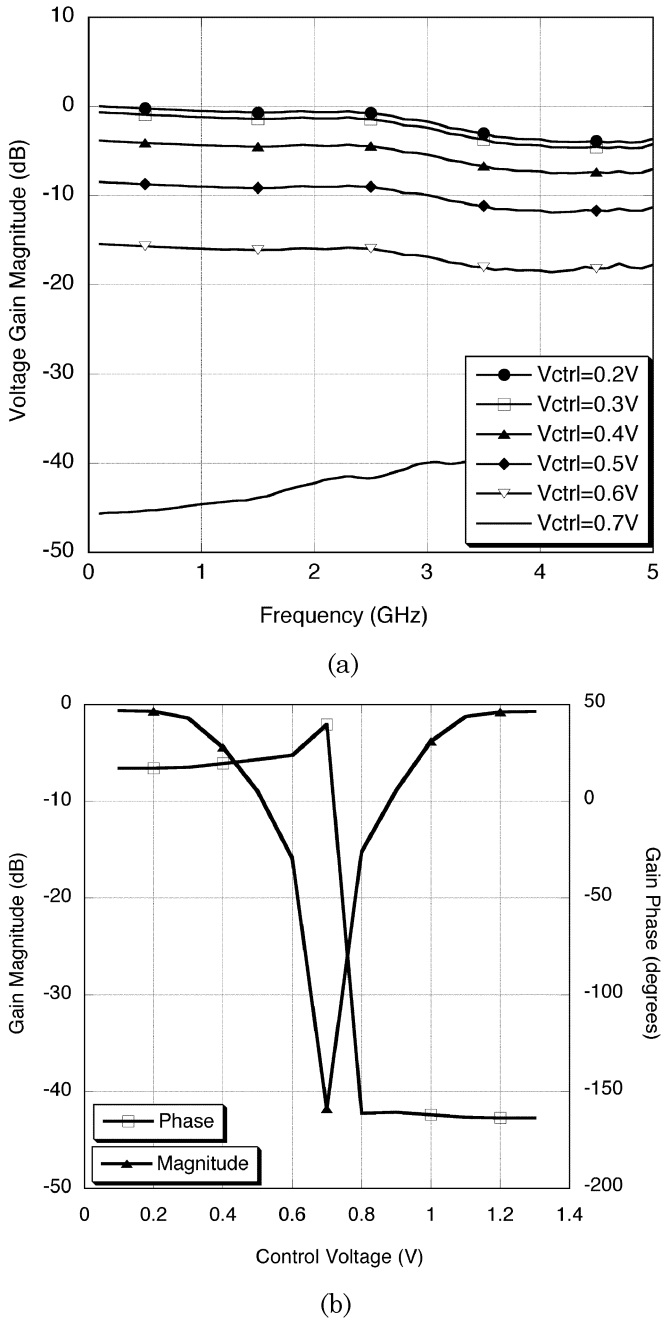

Fig. 8. (a) Variation of VGA gain magnitude with frequency. (b) Variation of VGA gain magnitude and phase with control voltage at 2.4 GHz.

against frequency. Fig. 8(b) shows a graph of gain and phase variation with control voltage in the 2.4-GHz band.

The phase aligner designed utilizes a delay interpolation technique [20]. Since the circuit fabricated employs active devices, it relies on delay manipulation to obtain phase shift. Such a configuration allows an excellent degree of continuous linear phase control over the entire range of 180°.

A 209-ps (approximately) range of controllable delay is, therefore, required of the rotator at the minimum frequency of interest. A block diagram describing the operating principle of the phase aligner is shown in Fig. 9(a), and some key blocks are expanded as schematics in Fig. 9(b) and (c).

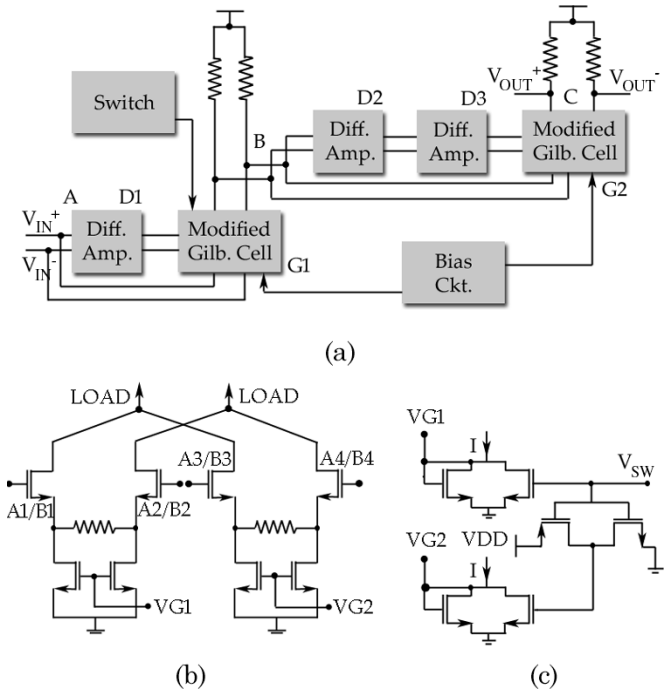

Fig. 9. (a) Simplified diagram showing phase shifter operation. (b) Circuit schematic of the modified Gilbert cell (G1 and G2). (c) Schematic of switching mechanism used to control G1 and toggle extra delay D1.

The portion of the circuit between B and C, as shown in Fig. 9(a) forms the core of the phase shifter. The modified Gilbert cell G2, which is expanded in Fig. 9(b), is configured such that each differential amplifier constituting the cell accepts a different set of inputs. Whereas one set of inputs arrives directly from B, the other is delayed by the two cascaded differential amplifiers (D2 and D3) between B and C. The cell G2 further sums the currents through each of its halves at the output node so that it effectively interpolates between the delays of its inputs.

The exact delay desired is obtained by adjusting the currents through the two halves of G2. This is done by means of a control voltage at the folded cascode current biasing circuit of G2 in a manner similar to the VGA.

With reference to Fig. 9(a), $\tau_{\rm BC}$ is the delay a signal experiences while propagating between B and C. This delay is variable and controlled by the current steering circuit that biases the modified Gilbert cell G2. It varies between $\tau_{\rm BC,min}$ and $\tau_{\rm BC,max}$ at the two extremes of the control range. Therefore, the total controllable delay range is

$$\Delta\tau_{\rm BC} = \tau_{\rm BC,max} - \tau_{\rm BC,min}. \tag{20}$$

Now, the differential amplifier delay cells D2 and D3 in Fig. 9(a) have fixed delays $\tau_{\rm D2}$ and $\tau_{\rm D3}$. The cell G2 interpolates between the two paths from B to C so that at one extreme of the control range, the output signal at C is entirely due to the fast path, and at the other, it is entirely due to the slow path through the D2 and D3. Hence, the controllable delay range in (20) above is

$$\Delta\tau_{\rm BC} = \tau_{\rm D2} + \tau_{\rm D3}. \tag{21}$$

The total gain of D2 and D3 must be unity so that the inputs to G2 differ only in phase but not in amplitude. However, despite ensuring the unity gain criterion, the nature of the interpolator prevents constant gain across the control range. One method of surmounting this is to use dynamic current biasing through the current source. If the tail current through G2 is increased nonlinearly through the middle of the bias range, a constant effective transconductance may be obtained. With nonlinear dynamic biasing through metal–oxide–semiconductor field-effect transistor (MOSFET) devices being difficult to achieve, this method is abandoned in favor of a simpler solution. Increasing the gain range of the VGA enough to ascertain that the total gain of the system is unity at the middle of the phase control range is sufficient.

The total delay range available from the above section of the circuit was around 150 ps, which corresponds to a phase range of 130° at 2.4 GHz. The section of the phase rotator circuit from A to B contributes the remainder of the phase control range. Again, this portion of the circuit consists of a modified Gilbert cell G1 that receives inputs directly from A and through the differential amplifier delay cell D1. G1 is different from G2 in that each of its differential amplifier halves is constant current biased. It does not operate by a current steering mechanism. The outputs are summed across the pair of matched load resistors at B. D1 is a unity gain stage providing more than 59 ps of delay. This is a fixed delay that can be turned on or off by a switching control circuit that biases the two halves of G1. The switching circuit is shown expanded in Fig. 9(c) and relies on an external digital voltage $V_{\rm SW}$, that takes values of 0 and 1.8 V. Therefore, if $\tau_{\rm AC0}$ and $\tau_{\rm AC1}$ represent the delay between A and C when D1 is switched off or on

$$\begin{aligned}\tau_{\rm AC0} &= \tau_{\rm G1} + \tau_{\rm BC}\\ \tau_{\rm AC1} &= \tau_{\rm D1} + \tau_{\rm G1} + \tau_{\rm BC}.\end{aligned} \tag{22}$$

However, the controllable delay range in each case is equal to $\Delta\tau_{\rm BC}$. The total delay range available over the two modes, which is also the total possible delay range of the entire circuit, is given by

$$\Delta\tau_{\rm AC} = \tau_{\rm AC,max} - \tau_{\rm AC,min} = \tau_{\rm D1} + \Delta\tau_{\rm BC} \tag{23}$$

which is more than the required 209 ps.

Another possible approach to designing the phase aligner is shown in Fig. 10.

This involves two independently controllable VGAs V_a and V_b with voltage gain ranges from 0 to 1 and a quadrature generation circuit. Assuming a sinusoidal input (ignoring modulation), if a and b are the gains of the two VGAs, and f the frequency of the input tone, the output is given by

$$y(t) = a\sin(2\pi ft) + b\cos(2\pi ft). \tag{24}$$

The output signal can be adjusted to have any amplitude from 0 to 1, and any phase shift from 0° to 360° with respect to the input, by appropriately varying a and b. The difficulty in this approach stems from the complexity involved in designing a precise high-frequency quadrature generator that functions across a frequency band.

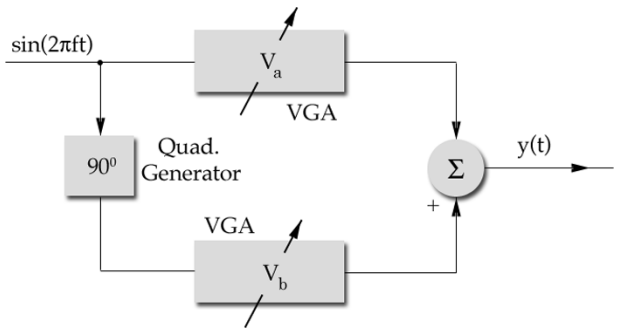

Fig. 10. Alternative scheme for the design of a variable phase shifter.

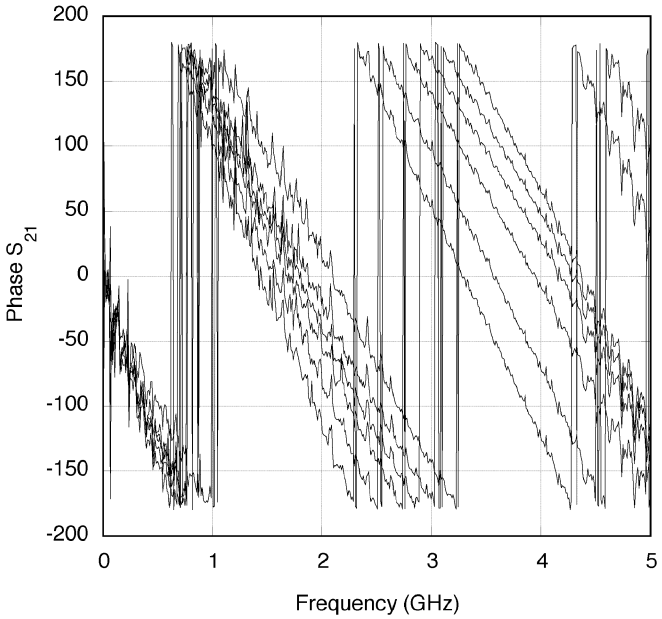

Fig. 11. Variation of the transmission phase with frequency for the phase aligner at different control voltages.

S-parameter and time-domain measurements were performed on the phase rotator fabricated. The measured phase variation at different frequencies as a function of control voltage is shown in Fig. 11. Phase wrapping is employed for ease of interpretation.

Generally speaking, for a modulated sinusoid being transmitted through a system with a bandpass characteristic, the carrier is delayed by the phase delay and the modulating data by the group delay. Eliminating phase dispersion, therefore, usually translates to a constant group delay or linear phase response requirement. This is reduced to a triviality in the context of the present problem because the bandwidth of interest (83.5 MHz) is very small compared to the center frequency (2.4 GHz). Independent control of the amplitude and phase necessitates a roughly constant gain characteristic for the phase shifter with varying control voltage. This, along with phase variation in-band is illustrated by the measurements shown in Fig. 12.

The bandpass emulation filter described earlier is adapted to the coupling channel. The varactor diode provides a tuning range of 2.1–2.6 pF controllable in steps of 0.1 pF, allowing a

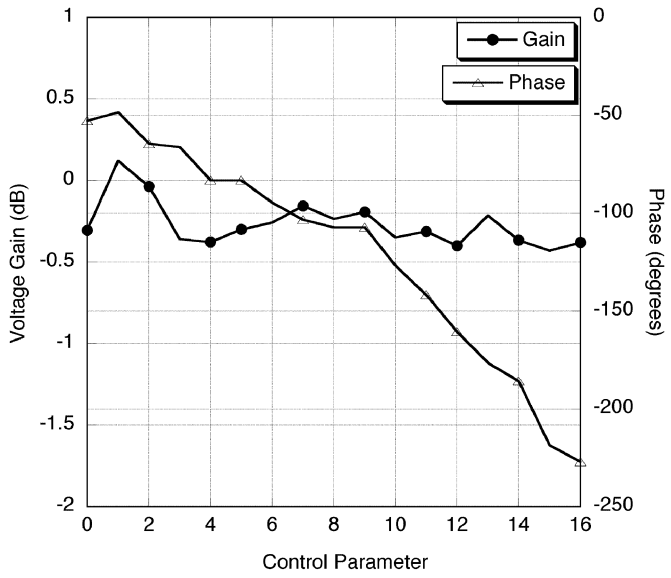

Fig. 12. In-band (2.4 GHz) variation of gain magnitude and phase with a control parameter for the phase shifter.

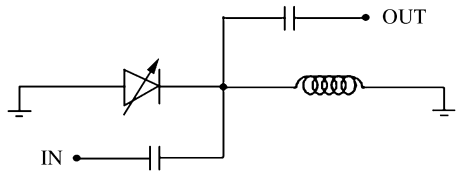

Fig. 13. Schematic of on-board tunable bandpass emulation filter.

wide range of filter Q factors. A schematic of the filter with limited tunability is shown in Fig. 13.

As the circuits that constitute the high-frequency path through the canceller are of a large delay type, the consequent resistance–capacitance (RC) time constants introduce many poles in the alternating current (ac) transfer function. Combined with the cascading of resistively loaded differential amplifier stages, this has the effect of reducing system ac bandwidth. Fortunately, the extremely narrow-band nature of the aggressor and the victim signals renders this effect inconsequential. The ac 6-dB voltage gain corner frequencies of the VGA and phase shifter were approximately 6 GHz and 600 MHz, respectively.

The transmission characteristics of the coupling channel, measured before and after cancellation, are shown in Fig. 14. A maximum cancellation of 30 dB is observed in-band, thereby reducing the interference level from -18 to -48 dB. When the antennas were arranged at a different distance, the coupling was decreased from -27 to -56.6 dB, implying a total cancellation of 29.6 dB. The null created, as noted from the graph, is narrower in bandwidth than may be desired. Appropriate tuning of the canceller produces a wider band null that provides a lower level of cancellation throughout the band, as noted in the previous section. These numbers directly translate to an SNR improvement in the victim receiver front-end. The total current consumption of the ICs is approximately 7.8 mA.

An active cancellation result reported in [16] shows improved isolation and reduced transmitter noise leakage into the receive band in a 2-GHz radio duplexer operating in a FDD scheme. A noise cancellation of up to 37 dB has been reported using

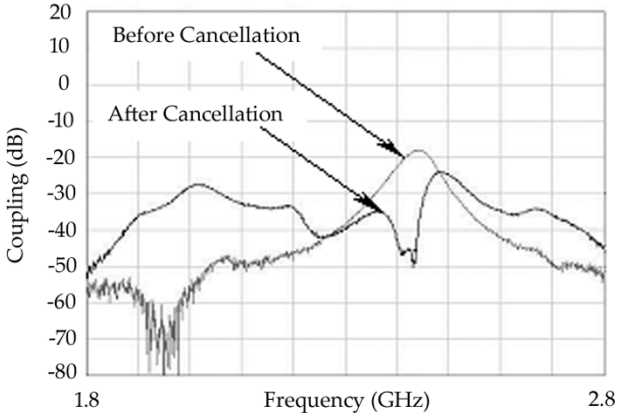

Fig. 14. Canceller performance showing magnitude of coupling before and after cancellation for one physical configuration of the aggressor and victim.

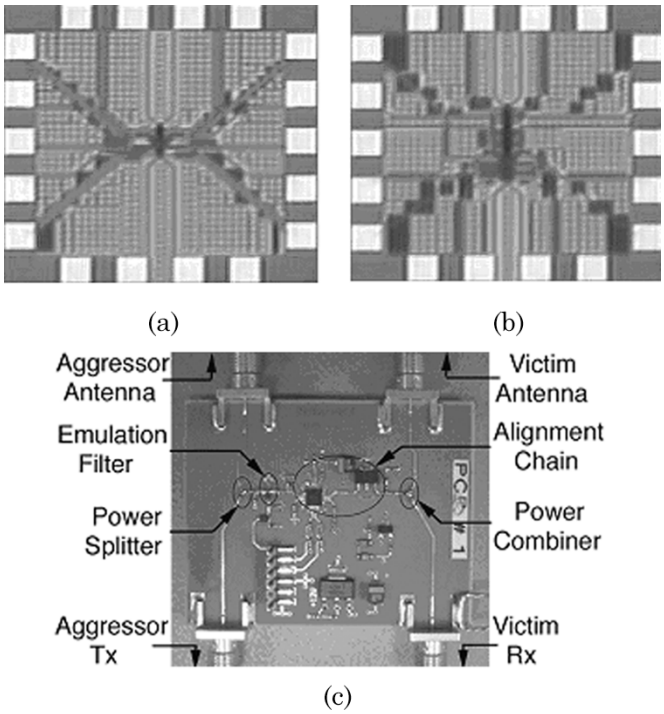

Fig. 15. (a) Microphotograph of VGA die for testing. (b) Microphotograph of phase aligner die for testing. (c) Photograph of canceller on evaluation board.

complex vector attenuators to establish double nulls. However, the narrow-band null created and the reference input source are at different frequencies and do not occupy the same band as in our problem. Photographs of some of the CMOS dice and the board are shown in Fig. 15.

V. Conclusion

An active cancellation technique enabling the coexistence of collocated radios has been analyzed. A canceller that provides significant interference mitigation at a low power cost has been designed. The general nature of the cancellation method proposed and implemented in this study suits its application to other radio environments provided the interfering radio systems are in close proximity of each other. Their mutual physical configuration also needs to be relatively static. These constraints are usually satisfied when the radios are situated on the same device. In the absence of the latter condition, or when the nature of correlation between the interferer and the reference signal is unknown, correlation must be established by means of an adaptive FIR filter. Relieving the extremely high-sensitivity GPS receiver of interference is a promising alternative application. Such interference is found to occur from the global system for mobile communications (GSM) (DCS 1800 MHz) transmitters that use power levels as high as 36 dBm operating in power class 3, or 30 dBm in power class 1 [21], in a frequency band 200 MHz away. In other devices, high-speed wire line baseband data transmissions in the vicinity of a GPS receiver may cause noise by spectral fallout.

Acknowledgment

The authors wish to acknowledge Quellan Inc., Atlanta, GA, for their collaboration and support in realizing the system.

References

[1] B. P. Crow, I. Widjaja, L. G. Kim, and P. T. Sakai, "IEEE 802.11 wireless local area networks," *IEEE Commun. Mag.*, vol. 35, no. 9, pp. 116–126, Sep. 1997.

[2] J. C. Haartsen, "The Bluetooth radio system," *IEEE Pers. Commun.*, vol. 7, no. 1, pp. 28–36, Feb. 2000.

[3] *Impact of Interference on the Bluetooth Access Control Performance: Preliminary Results*, IEEE Standard 802.15/00-322r0, 2000.

[4] *Impact of Bluetooth on 802.11 Direct Sequence*, IEEE Standard 802.11-98/319, 1998.

[5] *SCORT—An Alternative to the Bluetooth SCO Link for Operation in an Interference Environment*, IEEE Standard 802.15-01/145r0, 2001.

[6] J. Lansford, A. Stephens, and R. Nevo, "Wi-Fi (802.11b) and Bluetooth: Enabling coexistence," *IEEE Network*, vol. 15, no. 5, pp. 20–27, Sep.–Oct. 2001.

[7] C. F. Chiasserini and R. R. Rao, "Coexistence mechanisms for interference mitigation in the 2.4-GHz ISM band," *IEEE Trans. Wireless Commun.*, vol. 2, no. 5, pp. 964–975, Sep. 2003.

[8] I. Howitt, "WLAN and WPAN coexistence in UL band," *IEEE Trans. Veh. Technol.*, vol. 50, no. 4, pp. 1114–1124, Jul. 2001.

[9] R. V. Hogg and E. A. Tanis, *Probability and Statistical Inference*. New York: MacMillan, 1977.

[10] W. C. Jakes, *Microwave Mobile Communications*. New York: Wiley, 1974.

[11] *Extension of Bluetooth and 802.11 Direct Sequence Model*, IEEE Standard 802.11-98/378, 1998.

[12] T. S. Rappaport, *Wireless Communication Principles and Practice*. New York: IEEE Press, 1996.

[13] B. Widrow *et al.*, "Adaptive noise canceling: Principles and applications," *Proc. IEEE*, vol. 63, no. 12, pp. 1692–1716, Dec. 1975.

[14] B. Widrow and J. McCool, "A comparison of adaptive algorithms based on the methods of steepest descent and random search," *IEEE Trans. Antennas Propag.*, vol. AP-24, no. 5, pp. 615–637, Sep. 1976.

[15] A. Raghavan, E. Gebara, M. M. Tentzeris, and J. Laskar, "An active interference canceller for multistandard collocated radio," presented at the IEEE MTT-S Int. Microwave Symp., Long Beach, CA, Jun. 12–17, 2005.

[16] S. Kannangara and M. Faulkner, "Adaptive duplexer for multiband transceiver," in *Proc. Radio Wireless Conf.*, Boston, MA, Aug. 2003, pp. 381–384.

[17] G. Marsh and T. Sutton, "Analog active cancellation of a wireless coupled transmit signal," U.S. Patent 6 539 204, Mar. 25, 2003.

[18] S. Boll and D. Pulsipher, "Suppression of acoustic noise in speech using two microphone adaptive noise cancellation," *IEEE Trans. Acoust., Speech, Signal Process.*, vol. ASSP-28, no. 6, pp. 752–753, Dec. 1980.

[19] B. Widrow *et al.*, "Stationary and nonstationary learning characteristics of the LMS adaptive filter," *Proc. IEEE*, vol. 64, no. 8, pp. 1151–1162, Aug. 1976.

[20] B. Razavi, *Design of Analog CMOS Integrated Circuits*. New York: McGraw-Hill, 2001.

[21] *Digital Cellular Telecommunications System (Phase 2+, GSM): Radio Transmission and Reception*, ETSI Standard GSM05.05 Version 5.11.1 ETS 300 910, 1999.

Anand Raghavan (S'01) received the B.S. degree in electrical engineering from the Indian Institute of Technology, Madras, India, in 2001, the M.S. degree from the Georgia Institute of Technology, Atlanta, in 2003, and is currently working toward the Ph.D. degree at the Georgia Institute of Technology.

His research interests include RF IC design, device modeling, and IC design for high-speed and collaborative signal-processing applications.

Edward Gebara (M'05) received the B.S. (with highest honors), M.S., and Ph.D. degrees in electrical and computer engineering from the Georgia Institute of Technology, Atlanta, in 1996, 1999 and 2003, respectively.

He is currently a Member of Technical Staff with Quellan Inc., Atlanta, GA, where he develops high-performance analog semiconductors that improve the speed and reach of communication channels in consumer, broadcast, enterprise, computing and wireless markets. He is also a research faculty member with the Georgia Institute of Technology, where he leads the Mixed Signal Team research efforts. The team research interest is to develop the foundation for alternate modulation schemes (quadrature amplitude modulation (QAM), optical subcarrier multiplexing (OSCM), etc.), equalization techniques, and crosstalk cancellation techniques on pure CMOS applied to next-generation wired and wireless communication. He has authored or coauthored over 50 publications.

Emmanouil M. Tentzeris (SM'03) received the Diploma degree in electrical and computer engineering from the National Technical University of Athens, Athens, Greece, in 1992, and the M.S. and Ph.D. degrees in electrical engineering and computer science from The University of Michigan at Ann Arbor, in 1993 and 1998, respectively.

He is currently an Associate Professor with the School of Electrical and Computer Engineering, Georgia Institute of Technology, Atlanta. During the summer of 2002, he was a Visiting Professor with the Technical University of Munich, Munich, Germany. He has authored or coauthored over 170 papers in refereed journals and conference proceedings and eight book chapters. He has helped develop academic programs in highly integrated packaging for RF and wireless applications, microwave MEMS, system-on-package (SOP)-integrated antennas and adaptive numerical electromagnetics (finite difference time domain (FDTD), multiresolution algorithms). He is the Georgia Tech National Science Foundation (NSF)-Packaging Research Center Associate Director for RF Research and the RF Alliance Leader. He is also the Leader of the Novel Integration Techniques Sub-Thrust of the Broadband Hardware Access Thrust of the Georgia Electronic Design Center (GEDC) of the State of Georgia.

Dr. Tentzeris is member of the Technical Chamber of Greece. He was the 1999 Technical Program co-chair of the 54th ARFTG Conference, Atlanta, GA. He is the vice-chair of the RF Technical Committee (TC16) of the IEEE Components, Packaging, and Manufacturing Technology (CPMT) Society. He was the recipient of the 2003 IEEE CPMT Outstanding Young Engineer Award, the 2002 International Conference on Microwave and Millimeter-Wave Technology Best Paper Award (Beijing, China), the 2002 Georgia Tech-Electrical and Computer Engineering (ECE) Outstanding Junior Faculty Award, the 2001 ACES Conference Best Paper Award, the 2000 NSF CAREER Award, and the 1997 Best Paper Award, International Hybrid Microelectronics and Packaging Society.

Joy Laskar (S'84–M'85–SM'02–F'05) received the B.S. degree (highest honors) in computer engineering with math/physics minors from Clemson University, Clemson, SC, in 1985, and the M.S. and Ph.D. degrees in electrical engineering from the University of Illinois at Urbana-Champaign, in 1989 and 1991, respectively.

Prior to joining the Georgia Institute of Technology, Atlanta, in 1995, he held faculty positions with the University of Illinois at Urbana-Champaign and the University of Hawaii. At the Georgia Institute of Technology, he holds the Joseph M. Pettit Professorship of Electronics and is currently the Chair for the Electronic Design and Applications Technical Interest Group, the Director of Georgia's Electronic Design Center, and the System Research Leader for the National Science Foundation (NSF) Packaging Research Center. With the Georgia Institute of Technology, he heads a research group with a focus on integration of high-frequency electronics with opto-electronics and integration of mixed technologies for next-generation wireless and opto-electronic systems. In July 2001, he became the Joseph M. Pettit Professor of Electronics with the School of Electrical and Computer Engineering, Georgia Institute of Technology. He has authored or coauthored over 210 papers. He has ten patents pending. His research has focused on high-frequency IC design and their integration. His research has produced numerous patents and transfer of technology to industry. Most recently, his research has resulted in the formation of two companies. In 1998, he cofounded the advanced WLAN IC company RF Solutions, which is now part of Anadigics. In 2001, he cofounded the next-generation interconnect company Quellan Inc., Atlanta, GA, which develops collaborative signal-processing solutions for enterprise applications.

Dr. Laskar has presented numerous invited talks. For the 2004–2006 term, he has been appointed an IEEE Distinguished Microwave Lecturer for his Recent Advances in High Performance Communication Modules and Circuits seminar. He was a recipient of the 1995 Army Research Office's Young Investigator Award, 1996 recipient of the National Science Foundation (NSF) CAREER Award, 1997 NSF Packaging Research Center Faculty of the Year, 1998 NSF Packaging Research Center Educator of the Year, 1999 corecipient of the IEEE Rappaport Award (Best IEEE Electron Devices Society journal paper), the faculty advisor for the 2000 IEEE Microwave Theory and Techniques Society (IEEE MTT-S) International Microwave Symposium (IMS) Best Student Paper Award, 2001 Georgia Institute of Technology Faculty Graduate Student Mentor of the Year, a 2002 IBM Faculty Award, 2003 Clemson University College of Engineering Outstanding Young Alumni Award, and 2003 Outstanding Young Engineer of the IEEE MTT-S.